

Modeling river delta formation

Hansjörg Seybold ^{*}, José S. Andrade Jr. [‡] and Hans J. Herrmann ^{* ‡}

^{*}Computational Physics for Engineering Materials, IfB, ETH Zurich, 8093 Zurich, Switzerland, and [‡]Departamento de Física, Universidade Federal do Ceará, 60451-970 Fortaleza, Ceará, Brazil

Submitted to Proceedings of the National Academy of Sciences of the United States of America

A new model to simulate the time evolution of river delta formation process is presented. It is based on the continuity equation for water and sediment flow and a phenomenological sedimentation/erosion law. Different delta types are reproduced using different parameters and erosion rules. The structures of the calculated patterns are analyzed in space and time and compared with real data patterns. Furthermore our model is capable to simulate the rich dynamics related to the switching of the mouth of the river delta. The simulation results are then compared with geological records for the Mississippi river.

River Deltas | Simulation | Fractals | Lattice Model

Introduction

The texture of the landscape and fluvial basins is the product of thousands of years of tectonic movement coupled with erosion and weathering caused by water flow and climatic processes. To gain insight into the time evolution of the topography, a model has to include the essential processes responsible for the changes of the landscape. In Geology the formation of river deltas and braided river streams has been studied since a long time describing the schematic processes for the formation of deltaic distributaries and inter-levee-basins [1, 2, 3, 4, 5]. Experimental investigation of erosion and deposition has a long tradition in Geology [6]. Field studies have been carried out for the Mississippi Delta [7, 8, 9, 10], the Niger Delta [11, 12, 13], or for the Brahmaputra Delta [14]. Laboratory experiments have also been set up in the last decades for quantitative measurements [15, 16, 17, 18, 19, 20]. For instance, in the eXperimental EarthScape (XES) project the formation of river deltas is studied on laboratory scale and different measurements have been carried out [21, 22, 23].

Nevertheless modeling has proved to be very difficult as the system is highly complex and a large range of time scales is involved. To simulate geological time scales the computation power is immense and classical hydrodynamical models cannot be applied. Typically these models are based on a continuous *ansatz* (e.g., shallow water equations) which describes the interaction of the physical laws for erosion, deposition and water flow [24, 25, 26, 27, 28, 29]. The resulting set of partial differential equations are then solved with boundary and initial conditions using classical finite element or finite volume schemes. Unfortunately none of these continuum models is able to simulate realistic land-forms as the computational effort is much too high to reproduce the necessary resolution over realistic time scales. Therefore in the last years discrete models based on the idea of cellular automata have been proposed [30, 31, 32, 33, 34, 35]. These models consider water input on some nodes of the lattice and look for the steepest path in the landscape to distribute the flow. The sediment flow is defined as a nonlinear function of the water flow and the erosion and deposition are obtained by the difference of the sediment inflow and outflow. This process is iterated to obtain the time evolution. In contrast to the former models, these models are fast and several promising results have been obtained, but as they are only based on flow, a well defined water level cannot be obtained with this

ansatz.

Here we introduce a new kind of model where the water level and the landscape are described on a lattice grid coupled by an erosion and sedimentation law. The time evolution of the sediment and water flow is governed by conservation equations. The paper is organized as follows. After an overview on the different types of deltas and their classification the model is introduced and discussed in details. The analysis of the model results and a comparison with real land-forms are provided. According to different parameter combinations different delta types can be reproduced and interesting phenomena in the time evolution of a delta such as the switching of the delta lobe can be observed. Finally the scaling structure of the delta pattern is analyzed and compared with that obtained from satellite images.

Classification

The word “delta” comes from the Greek capital letter Δ and can be defined as a coastal sedimentary deposit with both subaerial and subaqueous parts. It is formed by riverborne sediment which is deposited at the edge of a standing water. This is in most cases an ocean but can also be a lake. The morphology and sedimentary sequences of a delta depend on the discharge regime and on the sediment load of the river as well as on the relative magnitudes of tides, waves and currents [36]. Also the sediment grain size and the water depth at the depositional site are important for the shape of the deltaic deposition patterns [1, 36, 37, 38]. This complex interaction of different processes and conditions results in a large variety of different patterns according to the local situations. Wright and Coleman [1, 36, 39, 40] described depositional facies in deltaic sediments and concluded that they result from a large variety of interacting dynamic processes (climate, hydrologic characteristics, wave energy, tidal action, etc.) which modify and disperse the sediment transported by the river. By comparing sixteen deltas they found that the Mississippi Delta is dominated by the sediment supply of the river while the Senegal Delta or the São Francisco River Delta are mainly dominated by the reworking wave activities. High tides and strong tidal currents are the dominant forces at the Fly River Delta.

Galloway [41] introduced a classification scheme where three main types of deltas are distinguished according to the dominant forces on the formation process: *river-*, *wave-* and *tide-*dominated deltas. This simple classification scheme was later extended [37, 38, 42] including also grain size and other effects.

At the river-dominated end of the spectrum, deltas are indented and have more distributaries with marshes, bays, or tidal flats in the interdistributary regions. They occur when the stream of the river and the resulting sediment transport is strong and other effects such as reworking by waves or by tides are minor [36, 39]. These deltas tend to form big delta lobes into the sea which may have little more than the distributary channel and its levee is exposed above the sea level.

Conflict of interest statement: No conflicts declared.

[†]To whom correspondence should be addressed. E-mail: hseybold@ethz.ch

©2007 by The National Academy of Sciences of the USA

Due to their similarity with a bird's foot, they are often referred in the literature as "bird foot delta" like in the case of the Mississippi River Delta [36]. When more of the flood plain between the individual distributary channels is exposed above the sea level, the delta displays lobate shape. Wave-dominated delta shorelines are more regular, assuming the form of gentle, arcuate protrusions, and beach ridges are more common (e.g., like for the Nile Delta or Niger Delta [12, 43]). Here the breaking waves cause an immediate mixing of fresh and salt water. Thus the stream immediately loses its energy and deposits all its load along the coast. Tide-dominated deltas occur in locations of large tidal ranges or high tidal current speeds. Such a delta often looks like a estuarine bay filled with many stretched islands parallel to the main tidal flow and perpendicular to the shore line (like e.g., the Brahmaputra Delta). Using the classification of Galloway [41] the different delta types of deltas can be arranged in a triangle where the extremes are put in the edges (see Fig. 1).

The Model

The model discretizes the landscape on an rectangular grid where the surface elevation H_i and the water level V_i are assigned to the nodes. Both H_i and V_i are measured from a common base point, which is defined by the sea level. On the bonds between two neighboring nodes i and j , a hydraulic conductivity for the water flow from node i to node j is defined as

$$\sigma_{ij} = c_\sigma \begin{cases} \frac{V_i + V_j}{2} - \frac{H_i + H_j}{2} & \text{if } > 0 \\ 0 & \text{else.} \end{cases} \quad [1]$$

As only surface water flow is considered, σ_{ij} is set larger than zero only if the water level of the source node is larger than the topography, which means that water can only flow out of a node where the water level is above the surface. The relation between the flux I_{ij} along a bond and the water level is given by

$$I_{ij} = \sigma_{ij}(V_i - V_j). \quad [2]$$

Furthermore water is routed downhill using the continuity equation for each node

$$\frac{V_i - V'_i}{\Delta t} = \sum_{N.N.} I_{ij}, \quad [3]$$

where the sum runs over all currents that enter or leave node i and V'_i is the new water level. The boundaries of the system are chosen as follows: On the sea side the water level on the boundary is set equally to zero and water just can flow out of the system domain. On the land the water is retained in the system by high walls or choosing the computational domain for the terrain such that the flow never reaches the boundary. Water is injected into the system by defining an input current I_0 at the entrance node.

The landscape is initialized with a given ground water table. Runoff is produced when the water level exceeds the surface. The sediment transport is coupled to the water flow by the rule, that all sediment that enters a node has to be distributed to the outflows according to the strength of the corresponding water outflow. Thus the sediment outflow currents for node i are determined via

$$J_{ij}^{out} = \frac{\sum_k J_{ik}^{in}}{\sum_k |I_{ik}^{out}|} I_{ij}^{out}, \quad [4]$$

where the upper sum runs over all inflowing sediment and the lower one over the water outflow currents. A sediment input current s_0 is defined in the initial bond.

The sedimentation and erosion process is modeled by a phenomenological relation which is based on the flow strength I_{ij} and the local pressure gradient imposed by the difference in the water levels in the two nodes V_i and V_j . The sedimentation/erosion rate dS_{ij} is defined through

$$dS_{ij} = c_1(I^* - |I_{ij}|) + c_2(V^* - |V_i - V_j|), \quad [5]$$

where the parameters I^* and V^* are erosion thresholds and the coefficients c_1 resp. c_2 determine the strength of the corresponding process. The first term $c_1(I^* - |I_{ij}|)$ describes the dependency on the flow strength I_{ij} [44] and is widely used in geomorphology, while the second term $c_2(V^* - |V_i - V_j|)$ relates sedimentation and erosion to the flow velocity, which in the model can be described by $I_{ij}/\sigma_{ij} \sim |V_i - V_j|$. The two terms of **5** are not linearly dependant on each other as one may think first by looking at Eq. **2**. In fact due to Eq. **1** there is a nonlinear relation between V and I which leads to different thresholds in the pressure gradient and the current.

The sedimentation rate dS_{ij} is limited by the sediment supply through J_{ij} , thus in the case $dS_{ij} > J_{ij}$ the whole sediment is deposited on the ground and J_{ij} is set to zero. In the other cases J_{ij} is reduced by the sedimentation rate or increased if we have erosion. The erosion process is also supply limited which means that the erosion rate is not allowed to exceed a certain threshold T ; so if $dS_{ij} < T$, then $dS'_{ij} = T$. Note that in the case of erosion dS_{ij} is negative. Due to erosion or deposition, the landscape is modified according to

$$H'_i = H_i + \frac{\Delta t}{2} dS_{ij} \quad [6]$$

$$H'_j = H_j + \frac{\Delta t}{2} dS_{ij}, \quad [7]$$

where the sediment deposits equally on both ends of the bond. The new topography is marked with H'_i . The same formulae (Eqs. **6**, **7**) also hold in the case of erosion when dS_{ij} is negative.

Iterating Eqns. **1** to **7** determines the time evolution of the system. Finally in a real system subaqueous water currents lead to a smoothening of the bottom which is modeled by the following expression

$$H'_i = (1 - \epsilon)H_i + \frac{\epsilon}{4} \sum_{N.N.} H_j, \quad [8]$$

where ϵ is a smoothening constant determining the strength of the smoothening process. The sum runs over all nearest neighbors of node i .

Simulation

The simulation is initialized with a valley on a rectangular $N \times N$ lattice with equal spacing grid as shown in Fig. 2. The valley runs downhill with slope S along the diagonal of the lattice and the hill-slopes of the valley increase from the bottom of the valley sideways according to a power law with exponent α . In the simulation shown in Fig. 3 the value of α was chosen to be 2.0. Under the sea the landscape is flat with a constant slope downhill. Furthermore we assume the initial landscape to have a disordered topography by assigning uniformly distributed random numbers to H_i . This variable is then smoothed out according to Eq. **8**. The water level V_i of the system is initialized with a given ground water table. In reality the distance of the ground water to the surface is minimal on the bottom of the valley and increases uphill. This is obtained in the simulation by choosing the water level V_i in an incline plane δ below the bottom of the valley. The slope of the plane is the same as the slope of the valley S . This also keeps the river close to the bottom of the valley. As we are only interested in studying the pattern formation at the mouth of the river,

the braiding conditions of the upper river only determine the width of the delta front. On the seaside when $H_i \leq 0$ the water level is a constant and set to zero. A sketch of the initial landscape is shown in Fig. 2.

An initial channel network is created by running the algorithm without sedimentation and erosion until the water flow reaches a steady state. Then the sedimentation and erosion procedure is switched on and the pattern formation at the mouth of the river is studied.

According to the dominance of the different processes, completely different coastline shapes can be observed. The smoothening procedure Eq. 8 leads to the formation of an estuary by reworking the coastline at the river mouth, while the stream dominant erosion term $c_1(I^* - |I_{ij}|)$ in Eq. 5 favors the formation of river-dominated birdfoot shaped delta. In contrast to this, the second term $c_2(V^* - |V_i - V_j|)$ in Eq. 5, which depends on the pressure gradient represented by the height difference of the water levels in the nodes i and j , produces more classical shaped deltas with several islands and channels. These patterns are similar to the distributary structure of the Lena or the Mahakam river delta, which are more sea or wave-dominated. This difference can be explained by the fact that the first term sediments along the main current stream, whereas the second term distributes the sediment more equally to the neighboring nodes.

Figures 3(a-c) show some snapshots of the time evolution of the simulation of a birdfoot delta ($c_2 = 0$). A map of the Mississippi River is given in Fig. 4 for comparison. In both cases one can see how the main channel penetrated into the ocean depositing sediment mainly on its levee sides. When the strength of the main channel decreases, side channels start to appear breaking through the sidebars as can be seen in the snapshots of Figs. 3(b) and 3(c). At the beginning of the delta formation process the sediment transport is equally distributed among the different channels and leads to a broader growth of the delta front along the coast. With time, the side channels are gradually abandoned and the sediment is primarily routed through the main channel, thus this dominant channel is growing faster than the others forming the typical birdfoot shaped deposits.

Figure 5(a) shows another type of delta where the smoothening of the waves reworks the deposits at the river mouth and distributes it along the coast. Here the river could built up only a slight protrusion in the immediate vicinity of the river mouth. The same happens in areas where the wave currents are dominant and lead to the formation of wave-dominated deltas like the São Francisco River in Brazil or the Nile Delta. A map of the São Francisco River Delta is also given in Fig. 5(b) for comparison. Here the coast line has been straightened by the wave activities and consists almost completely of beach ridges which have the typical triangular shape inland. This flattened deposit can also be found in our simulation results. As there is no evaporation included in the simulation, small ponds and abandoned channels remain in the sedimented zone instead of disappearing with time.

Finally, if the term $c_2(V^* - |V_i - V_j|)$ dominates the sedimentation/erosion process a half moon shaped delta with many small islands and channels appear. This delta type shows more activity in the channel network than the others. The channels split and come together, and when the main channel blocks its way due to sedimentation, the whole delta lobe switches to another place. This phenomenon is called delta switching. During the simulation, the switching of the delta occurred several times.

The best studied delta in the world is that of the Mississippi river where the switching of the delta lobes was studied in detail [8]. The switching of the Mississippi Delta during the last 4000 years is well documented [7, 8, 45]. The rich dynamics due to the switching phe-

nomenon that is observed in the Mississippi can be also identified in our simulations. In the literature [36] three types of switching mechanisms are distinguished. The first type referred as switching type I, consists of a lobe switching in which the delta propagates in a series of distributary channels. After a certain time, the stream abandons the entire system close to the head of the delta and forms a new lobe in an adjacent region. Very often this lobe occupies an indentation in the coastline between previous existing lobes so that with time the sediment layers overlap each other. One can find this type of delta switching in areas where the offshore slope is extremely low and the tidal and wave forces are too small for reworking the lobe [36, 39, 41]. In many cases the delta lobes merge with each other forming major sheet-type sand banks. This phenomena can be nicely observed when comparing the two images of the simulation in Figs. 6(a) and 6(b). In the Mississippi Delta this also happened several times in the past and the different lobes have today different names. A type I shift of the Mississippi delta occurred for example, 4600 years B.C. between the Salé-Cypremort and the Cocodrie (4600-3500) Lobe or when the St. Bernard Lobe switched to which today is called Lafourche at about 1000 BC.

At about 3500 BC the Mississippi river switched far upstream from the Cocodrie to the Teche stream tailing a completely new course for the river itself and its delta. This type of switching is referred as type II switching [36] and can also be found in the simulation. When comparing Figs. 6(b) and 6(c) one can see a major shift of the channel far upstream in the deltaic plain so the river takes a completely different course and forms a new delta beside.

The type III of delta switching is referred in the literature as alternate channel extension [36]. In this case not the complete channel but the dominance of sediment flux in one or more distributaries is changing with time. This can be described as follows: two or more major channels split into several distributaries nearly at the same point at the head of the delta. Commonly one of the distributaries is dominant, so it will carry most of the sediment and water discharge at any time. As a result, this active channel will rapidly propagate seaward, while the other channel will shrivel with time. At some point, the slope of the main active channel will decrease and the discharge will seek one of the shorter distributaries. With the increased sediment flux downstream, the new channel will rapidly propagate into the sea. This switching process will repeat several times forming a deltaic plain characterized by a series of multiple beach ridges. This type of switching can be best observed in the simulation of the birdfoot delta in Fig. 3(a-c), where the main path of the sediment flow is marked by the red arrows. One can see how side channels emerge and are abandoned after a certain time. Nevertheless, a major switching of the main channel could not be observed in the simulations. The average time between two lobe switchings was found to be around 1000 years for the Mississippi river [8, 36, 45].

At this point, we show that the river delta patterns generated from our simulations display geometric features that are statistically similar to real river delta structures. More precisely, we analyze the self similar behavior of the real and simulated river deltas using the box counting algorithm [46]. The box counting dimension is a quite common measure in geomorphological pattern analysis and has been used by many authors to characterize river basin patterns and coastlines [47, 48, 49].

For the real satellite picture as well as for the simulated river delta, we show in Figs. 7 that the variation with the cell size s of the number of cells N covering the land follows typical power laws over more than 3 decades

$$N \sim s^{-D}, \quad [9]$$

where the exponent D is the fractal dimension. Moreover, the least square fit of this scaling function to the data gives exponents which are strikingly close to each other, namely $D = 1.81 \pm 0.01$ for the real Lena river delta and $D = 1.85 \pm 0.1$ for the simulation.

Conclusion

A new model for simulating the formation process of river deltas has been presented. It is based on simple conservation laws for water and sediment on a lattice grid, coupled by a phenomenological sedimentation/erosion law. Several interesting features of river deltas like the

different delta switching processes could be found with the model and compared with real landforms.

Different delta shapes in the classification scheme of Galloway [41] could be reproduced by varying the model parameters and initial conditions. The pattern structure of the simulation has been analyzed and good agreement with real deltas have been found. Furthermore the delta shifting phenomena could be observed in the simulation and different types of delta shifting could be distinguished.

This work was funded by the Swiss National Fond and the Max Planck Prize as well as by the Landesstiftung BW, CNPq, CAPES and FUNCAP.

1. Coleman, J & Wright, L. (1975) *Modern river deltas: variability of processes and sand bodies* ed. Broussard, M. (Houston Geological Society), pp. 99–149.
2. Allen, G, Laurier, D. & Thouvenin, J. P. (1981) *A.A.G.P. Bull.* **65**, 889–889.
3. Coleman, J. (1988) *Geol. Soc. Am. Bull.* **100**, 999–1015.
4. Bridge, J. (1993) in *Braided Rivers*, ed. Bristow, C. (Geol. Soc., London), pp. 13–71.
5. Bristow, C & Best, J. (1993) in *Braided Rivers*, ed. Bristow, C. (Geol. Soc., London), pp. 1–11.
6. Jaggard, T. A. (1908) *Bull. Mus. Compar. Zool.* **49**, 285–305.
7. Fisk, H. (1947) Fine-grained alluvial deposits and their effects on mississippi river activities, (U.S. Army Corps of Engineering, Mississippi River Commission), Technical report. <http://lmvmapping.ercdc.usace.army.mil/>.
8. Kolb, C. R & Lopik, J. v. (1958) Geology of the mississippi deltaic plain, southeastern louisiana, (U.S. Army Corps of Engineering, Waterways Experiment Station), Technical report.
9. Coleman, J & Gagliano, S. (1964) *Gulf Coast Assn. Geol. Soc. Trans.* **14**, 67–80.
10. Could, H. (1970) *The Mississippi Delta complex* ed. Morgan, J. (Soc. of Economic Paleontologists and Mineralogists Special Publication), Vol. 15, pp. 3–30.
11. Allen, G. (1964) *Mar. Geol.* **1**, 289–332.
12. Allen, G. (1965) *Geol. en Mijnb* **44**, 1–21.
13. Allen, G. (1970) *Sediments of the modern Niger Delta* ed. Morgan, J. pp. 138–151.
14. Coleman, J. (1969) *Sediment. Geol.* **5**, 39–57.
15. Czirik, A & Somfai, E. (1993) *Phys. Rev. Lett.* **71**, 2154–2157.
16. Ashmore, P. (1982) *Earth Surf. Proc. Land.* **7**, 201–225.
17. Ashmore, P. (1985) Ph.D. thesis (University of Alberta, Alberta).
18. Wright, S & Parker, G. (2005) *J. Hydr. Res.* **43**, 612–630.
19. Parker, G. (2005) Sediment transport morphodynamics, with applications to fluvial and subaqueous fans and fan-deltas (edited, copyrighted e-book).
20. Parker, G, Toro-Escobar, M, Ramey, M, & Beck, S. (2003) *J. Hydraul. Eng.* **129**, 885–895.
21. Kim, W, Paola, C, Voller, V, & Swenson, J. (2006) *J. Sediment. Res.* **76**, 270–283.
22. Swenson, C, Paola, C, Pratson, L, Voller, V. R, & Murray, A. B. (2005) *J. Geophys. Res.* **110**, 1–16.
23. Lague, D, Crave, A, & Davy, P. (2003) *J. Geophys. Res.* **108**. doi: 10.1029/2002JB001785.
24. Giacometti, A, Maritan, A, & Banavar, J. (1995) *Phys. Rev. Lett.* pp. 577–580.
25. Willgoose, G, Bras, R, & Rodriguez-Iturbe, I. (1991) *Water Resour. Res.* **27**, 1671–1684.
26. Howard, A. D. (1994) *Water Resour. Res.* **30**, 2261–2285.
27. Kooi, H & Beaumont, C. (1996) *J. Geophys. Res.* **101**, 3361–3386.
28. Densmore, A, Anderson, R, McAdoo, B, & Ellis, M. (1997) *Science* **275**, 369–372.
29. Beaumont, C, Kooi, H, & Willett, C. (2000) *Coupled tectonic-surface process models with applications to rifted margins and collisional orogens* ed. Summerfield, M. (Wiley), pp. 29–55.
30. Wolfram, S. (2002) *A new kind of science*. (Wolfram Media Inc., Champaign, Illinois, USA).
31. Murray, A & Paola, C. (1994) *Nature* **371**, 54–57.
32. Murray, A & Paola, C. (1997) *Earth. Surf. Proc. Land.* **22**, 1001–1025.
33. Darvy, P & Carve, A. (2000) *Phys. Chem. Earth* **25**, 533–541.
34. Coulthard, T. J. (2005) *Water Resour. Res.* **41**, 04003, doi:10.1029/2004WR003201.
35. Coulthard, T. J & van de Vel, M. J. (2006) *Earth. Surf. Proc. Land.* **31**, 123–132.
36. Coleman, J. (1975) *Deltas: Processes of Deposition and Models for Exploration*. (Continuing Education Publication Company, Inc., Campaign, IL).
37. Bhattacharya, J. P & Walker, R. G. (1992) in *Facies Models, Response to Sea-Level Change*, eds. Walker, R. G & James, N. (Geological Association of Canada, St. Johns), pp. 157–177.
38. Orton, G. J & Reading, H. G. (1993) *Sedimentology* **40**, 475–512.
39. Wright, L. D & Coleman, J. M. (1973) *A.A.P.G. Bull.* **57**, 370–398.
40. Coleman, J & Wright, L. (1973) *Trans. Gulf Coast Assoc. Geol. Soc.* **23**, 33–36.
41. Galloway, W. (1975) *Process framework for describing the morphologic and stratigraphic evolution of deltaic depositional systems* ed. Broussard, M. (Houston Geological Society), pp. 87–98.
42. Wright, L. (1985) in *River deltas. Coastal Sedimentary Environments*, ed. Davis, R. A. J. (Springer-Verlag, New York), pp. 1–76.
43. Oomkens, E. (1974) *Sedimentology* **21**, 145–222.
44. Wipple, K & Tucker, G. (1999) *J. Geophys. Res.* **104**, 17661–17667.
45. Fisk, H. (1952) Geological investigation of the atchafalaya basin and the problem of mississippi river diversion, (U.S. Army Corps of Engineering, Mississippi River Commission), Technical report. <http://lmvmapping.ercdc.usace.army.mil/>.
46. Feder, J. (1989) *Fractals*. (Plenum Press, New York), 4 edition.
47. A. Maritan, A, Colaiori, F, Flammini, A, Cieplak, M, & Banavar, J. (1996) *Science* **272**.
48. Rodriguez-Iturbe, I & Rinaldo, A. (1997) *Fractal River Basins: Chance and Self-Organization*. (Cambridge University Press, New York).
49. Sapoval, B, Baldassarri, A, & Gabrielli, A. (2004) *Phys. Rev. Lett.*



Fig. 1. The figure shows the classification scheme after Galloway [41], where wave- tide- and river-dominated deltas are distinguished in the extremes of the triangle. By comparing 16 major river deltas Wright & Coelman [39] concluded that in the extremes the Mississippi is the most river-dominated delta and the São Francisco the most wave-dominated one. The delta which is mainly dominated by the tides is that of the Fly river in Papua New Guinea.

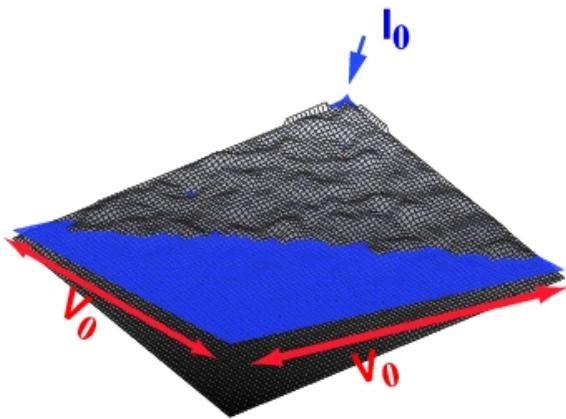


Fig. 2. The figure shows a sketch of the initial condition for a simulation. A water current I_0 is injected at the upper node and the water levels on the sea boundaries are kept constant ($V_0 = 0$). The landscape is initialized as an inclined plane with a disordered topography on the top. The water surface (blue) is parallel to the horizontal plane.

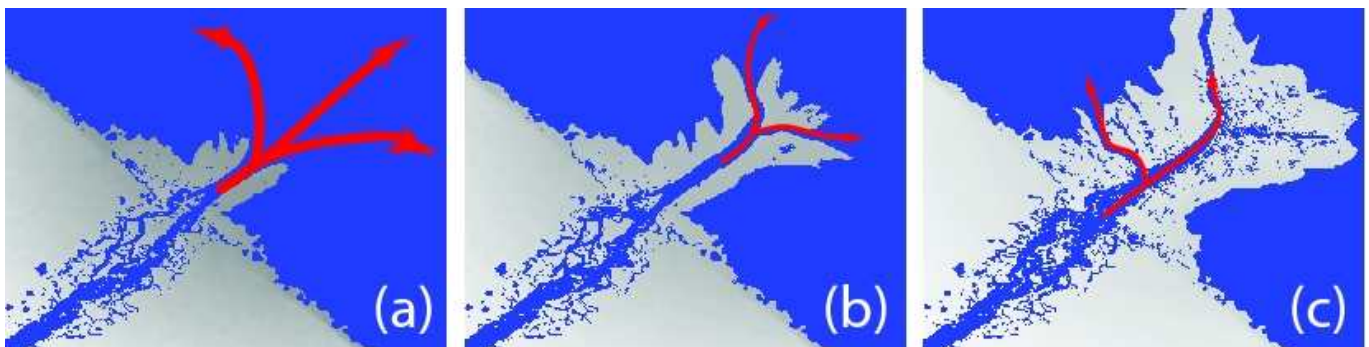


Fig. 3. Time evolution of a birdfoot delta (from left to right). Figure (a) shows the delta after 1.2 million time steps, where the main channel worked into the sea depositing sediment mainly on its levee sides. After 2.5 million time steps the main channel has split into two distributaries (b), where the smaller one becomes inactive after 5 million steps and a new channel breaks through the sidewalls (c). The main directions of the sediment flow are marked with the red arrows. The simulation was run on a 279×279 lattice and the parameters for the water flow were $I_0 = 1.7 \times 10^{-4}$ and $c_\sigma = 8.5$. For the sedimentation and erosion the constants were set to $c_1 = 0.1$ and $c_2 = 0$ with a sediment input current of $s_0 = 0.00025$. The erosion threshold I^* was set to $I^* = 4 \times 10^{-6}$ and the maximal erosion rate was set to $|T| = 5 \times 10^{-7}$. Smoothing was applied every 2000 time steps with a smoothing factor of $\epsilon = 1 \times 10^{-4}$. The initial depth of the water table at the bottom of the valley was set to $\delta = 0.0025$.



Fig. 4. For comparison with the simulation results of Fig. 3 the figure shows part of a map of the mouth of the Mississippi river, where the birdfoot shaped delta can be seen clearly. The colors indicate channel deposits (dark green), sand ridges (light green), swamps (medium green) and marshes (dark green). The figure was generated after [36].

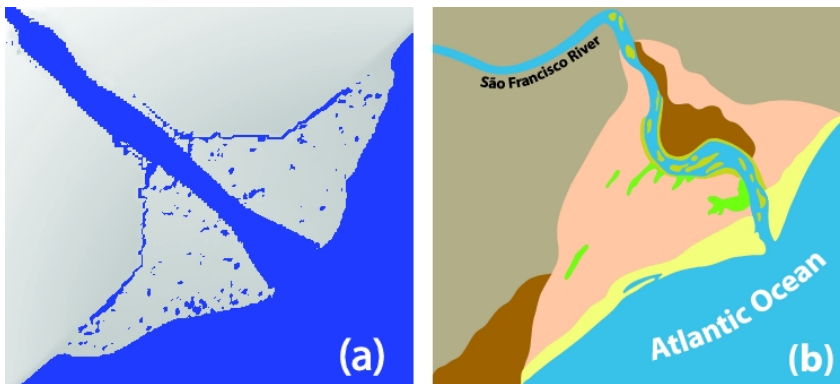


Fig. 5. In (a) the simulation of a wave-dominated delta is shown. While the waves are reworking the coast at the mouth of the river to form an estuary, the river deposits sediment and forms large beaches. As the simulation does not include evaporation, the ponds and inactive channels in the deposition zone do not disappear as in the map of the real river shown in (b). The parameters in the simulation were $N = 179$, $I_0 = 1.7 \times 10^{-4}$, $s_0 = 0.0015$, $c_\sigma = 8.5$, $c_1 = 0$, $c_2 = 0.1$ and $I^* = 1.3 \times 10^{-4}$. Smoothing was applied every 200 time steps with a smoothing constant $\epsilon = 0.01$. In (b) we show for comparison a map of the São Francisco river delta in southern Brazil which is the most wave-dominated delta according to the classification of [41]. The colors in the map (Fig. (b)) indicate channel deposits (dark green), beach ridges (orange), eolian dunes (yellow), marsh-mangroves (light green), the floodplain (brown) and the uplands (grey). The figure was generated after [36].

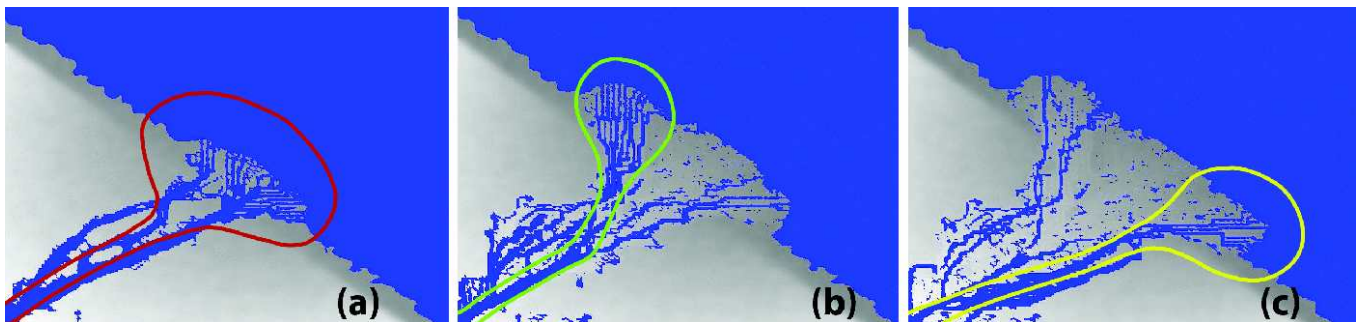


Fig. 6. The figures show the switching of the delta lobe during the simulation. Comparing Figs. (a) and (b) a type I switching can be identified where the main part of the delta lobe is abandoned close to the mouth of the river just before the river splits into several distributaries and forms a new lobe beside. Another type of delta switching is shown comparing Figs. (b) and (c) with two snapshots from the simulation. Here the channel switches far upstream and takes a new course to the coast forming another delta lobe far away. This is referred as a switching of type II. The parameters for the simulation were $I_0 = 1.7 \times 10^{-4}$, $s_0 = 5 \times 10^{-5}$, $c_2 = 0.0005$, $c_1 = 0$ and $I^* = 3.3 \times 10^{-4}$. The simulation was run on a 179×179 lattice with smoothing every 2000 time steps and a smoothing constant of $\epsilon = 0.0001$.

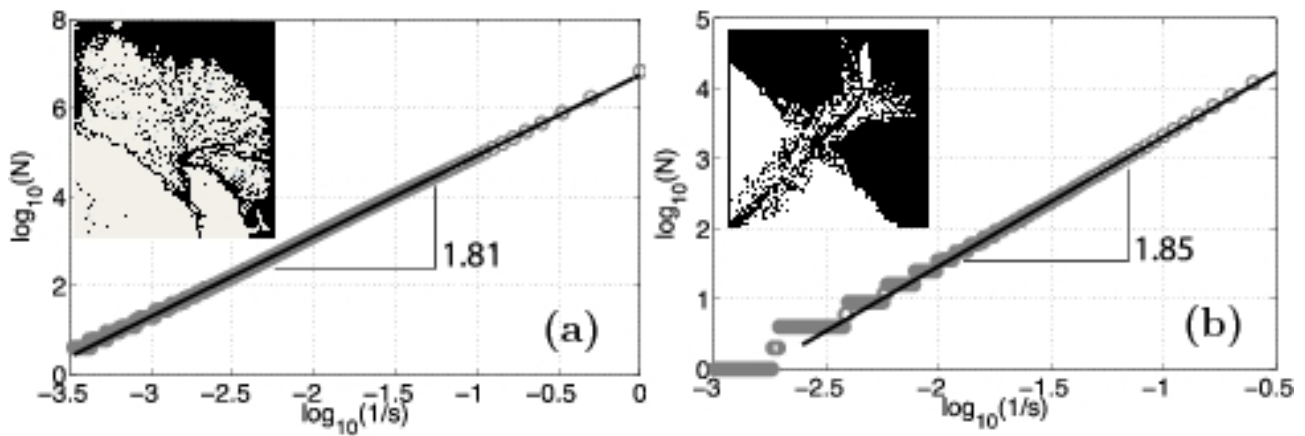


Fig. 7. Figure (a) shows the scaling behavior of the Lena river delta. On the y-axis we show the logarithm of the number of boxes $N(s)$ of size s which are necessary to cover the subaerial surface is plotted versus the logarithm of the inverse box size. The straight line is a power law fit $N \sim s^{-D}$ with exponent $D = 1.81$. In the inset a satellite picture of the Lena delta is shown. In (b) one can see the scaling behavior of the birdfoot delta from the simulation (c.f. Fig. 3) where the slope was calculated to be 1.85.